the fluctuations in our measurements were random in time and, in many cases, suggested bistability with leakage current moving between two stable values. We discuss the origin of such fast bistable fluctuations in the supporting text.

The ensemble of random nuclear spins that gives rise to the mixing of two-electron states as observed in this experiment also gives rise to an uncertainty of $g\mu_B \sqrt{\langle {B_N}^2 \rangle} = 0.03$ μeV in the Zeeman splitting of one electron. When averaged over a time longer than the correlation time of the nuclear spin bath (~100 μs) (*27*), this implies an upper limit on the time-averaged spin coherence time of $T_2^* = (\frac{\hbar}{2\pi})/g\mu_B\sqrt{\langle \frac{2}{3}{B_N}^2 \rangle} = 25$ ns [as defined by Merkulov *et al.* (*4*)], comparable to the T_2^* found in recent optical spectroscopy measurements (*28*). This value is four orders of magnitude shorter than the theoretical prediction for the electron spin T_2 in the absence of nuclei, which is limited only by spin-orbit interactions (*29*–*31*).

One way to eliminate the uncertainty in Zeeman splitting that leads to effective dephasing is to maintain a well-defined nuclear spin polarization (*12*). Many of the regimes explored in this paper show leakage current that is stable when current-induced polarization is allowed to settle for some time. These may in fact be examples of specific nuclear polarizations that are maintained electrically.

References and Notes

1. F. Meier, B. P. Zakharchenya, Eds., *Optical Orientation* (North-Holland, New York, 1984).
2. D. Gammon *et al.*, *Science* **277**, 85 (1997).
3. D. Loss, D. P. DiVincenzo, *Phys. Rev. A.* **57**, 120 (1998).
4. I. A. Merkulov, A. L. Efros, J. Rosen, *Phys. Rev. B* **65**, 205309 (2002).
5. P.-F. Braun *et al.*, *Phys. Rev. Lett.* **94**, 116601 (2005).
6. A. S. Bracker *et al.*, *Phys. Rev. Lett.* **94**, 047402 (2005).
7. M. Eto, T. Ashiwa, M. Murata, *J. Phys. Soc. Jpn.* **73**, 307 (2004).
8. B. E. Kane, *Nature* **393**, 133 (1998).
9. J. M. Taylor, A. Imamoglu, M. D. Lukin, *Phys. Rev. Lett.* **91**, 246802 (2003).
10. J. Schliemann, A. Khaetskii, D. Loss, *J. Phys. Condens. Matter* **15**, R1809 (2003).
11. A. V. Khaetskii, D. Loss, L. Glazman, *Phys. Rev. Lett.* **88**, 186802 (2002).
12. W. A. Coish, D. Loss, *Phys. Rev. B* **70**, 195340 (2004).
13. W. G. van der Wiel *et al.*, *Rev. Mod. Phys.* **75**, 1 (2003).
14. K. Ono, D. G. Austing, Y. Tokura, S. Tarucha, *Science* **297**, 1313 (2002).
15. A. C. Johnson, J. R. Petta, C. M. Marcus, M. P. Hanson, A. C. Gossard, *cond-mat*/0410679 (2004).
16. The electrostatic gates are on the surface of a GaAs/AlGaAs heterostructure. The two-dimensional electron gas is 90 nm below the surface, with density 1.33×10^{11} cm^{-2} and mobility 9.71×10^5 cm^2/Vs. Measurements were performed in a dilution refrigerator at 150 mK, with a magnetic field in the plane of the heterostructure.
17. D. Paget, G. Lampel, B. Sapoval, V. I. Safarov, *Phys. Rev. B* **15**, 5780 (1977).
18. D. Gammon *et al.*, *Phys. Rev. Lett.* **86**, 5176 (2001).
19. T. Fujisawa *et al.*, *Science* **282**, 932 (1998).
20. O. N. Jouravlev, Y. Nazarov, personal communication.
21. The difference between the field dependence of the resonant and inelastic currents can be explained by the coupling with the leads. The S(0,2) state is lifetime-broadened because of coupling with the right lead (~0.3 μeV), giving a weaker field dependence for the resonant current. The field dependence of the inelastic leakage is not affected by the lead coupling, because under the high-bias conditions of this experiment, there were no available states in the left lead that could broaden S(1,1).
22. A. C. Johnson *et al.*, *Nature* **435**, 925 (2005).
23. M. Dobers, K. v. Klitzing, J. Schneider, G. Weimann, K. Ploog, *Phys. Rev. Lett.* **61**, 1650 (1988).
24. A. K. Hüttel *et al.*, *Phys. Rev. B* **69**, 073302 (2004).
25. The leakage current is sensitive to magnetic fields of only a few mT, corresponding to 0.1% nuclear polarization. Given that the dot has ~10^6 nuclei, changes in the nuclear polarization of 0.1% can be caused by 1000 electron-nuclear flip-flop processes. For typical currents (~100 fA), 1000 electrons move through the dot in 1 ms, so in principle current fluctuations as fast as 1 kHz are possible.
26. K. Ono, S. Tarucha, *Phys. Rev. Lett.* **92**, 256803 (2004).
27. R. de Sousa, S. Das Sarma, *Phys. Rev. B* **67**, 033301 (2003).
28. Bracker et al. (*6*) found a T_2^* of 16 ns in a GaAs quantum dot, slightly shorter than in our experiment, presumably because of a smaller dot size. Braun et al. (*5*) measured a considerably shorter time scale, 500 ps, in InAs dots, because of a notable difference in dot size, nuclear spin *I*, and the stronger hyperfine coupling constant in InAs.
29. V. N. Golovach, A. V. Khaetskii, D. Loss, *Phys. Rev. Lett.* **93**, 016601 (2004).
30. J. M. Elzerman *et al.*, *Nature* **430**, 431 (2004).
31. M. Kroutvar *et al.*, *Nature* **432**, 81 (2004).

32. We thank O. N. Jouravlev and Y. Nazarov for developing a model that helped greatly with the physical interpretation of the data; G. Burkard, W. A. Coish, V. N. Golovach, A. C. Johnson, D. Loss, and C. M. Marcus for fruitful discussions; R. Schouten, B. van den Enden, and M. van Oossanen for technical assistance; and J. Caro for supporting infrastructure. Supported by the Defense Advanced Research Projects Agency Quantum Information Science and Technology program, the Dutch Organization for Fundamental Research on Matter (FOM), the Netherlands Organization for Scientific Research (NWO), the Office of Naval Research, Exploratory Research for Advanced Technology, and the EU Research Training Network on spintronics.

Supporting Online Material

www.sciencemag.org/cgi/content/full/1113719/DC1
SOM Text
Figs. S1 to S3
References and Notes

18 April 2005; accepted 12 July 2005
Published online 21 July 2005;
10.1126/science.1113719
Include this information when citing this paper.

Gas Adsorption Sites in a Large-Pore Metal-Organic Framework

Jesse L. C. Rowsell,[1] Elinor C. Spencer,[2] Juergen Eckert,[3,4] Judith A. K. Howard,[2] Omar M. Yaghi[1]*

The primary adsorption sites for Ar and N_2 within metal-organic framework-5, a cubic structure composed of $Zn_4O(CO_2)_6$ units and phenylene links defining large pores 12 and 15 angstroms in diameter, have been identified by single-crystal x-ray diffraction. Refinement of data collected between 293 and 30 kelvin revealed a total of eight symmetry-independent adsorption sites. Five of these are sites on the zinc oxide unit and the organic link; the remaining three sites form a second layer in the pores. The structural integrity and high symmetry of the framework are retained throughout, with negligible changes resulting from gas adsorption.

Metal-organic frameworks (MOFs) have recently emerged as an important class of porous materials for their amenability to design and the flexibility with which their pores can be functionalized (*1*–*3*). In particular, their extraordinary low density (1.00 to 0.20 g/cm^3) and high surface area (500 to 4500 m^2/g) make them ideal candidates for the storage and separation of gases (N_2, Ar, CO_2, CH_4, and H_2) (*4*–*12*). In this context, identifying the gas adsorption sites in MOFs is critically important to our ability to fine-tune those sites, sterically and electronically, in order to achieve the maximum storage capacity and selectivity.

Precise determination of adsorption sites in large-pore materials remains an ongoing challenge, because the characterization techniques that are commonly applied to this problem, such as inelastic neutron scattering (INS) and diffuse reflectance infrared spectroscopy, do not provide adequate information on the structural details of the adsorption sites (*9*, *13*). The recent powder x-ray diffraction (XRD) studies of gases in MOFs (*14*, *15*) do not elucidate the nature of adsorption sites because the MOFs used have very small pores and lack the possibility of adsorbing gases on multiple sites. For large-pore structures, a more precise technique is required to determine whether adsorption sites lie on the metal oxide or the organic moieties, how many exist, and precisely where they are located in the MOF structure.

We report the detailed single-crystal XRD study of Ar and N_2 adsorbed on the internal surface of a large-pore open-framework mate-

[1]Materials Design and Discovery Group, Department of Chemistry, University of Michigan, 930 North University Avenue, Ann Arbor, MI 48109, USA. [2]Department of Chemistry, University of Durham, South Road, Durham DH1 3LE, UK. [3]Materials Research Laboratory, University of California, Santa Barbara, CA 93106, USA. [4]Los Alamos Neutron Science Center–12, Mail Stop H805, Los Alamos National Laboratory, Los Alamos, NM 87545, USA.

*To whom correspondence should be addressed. E-mail: oyaghi@umich.edu

rial, MOF-5 (*4*). We were able to identify the metrics and geometry of five different primary adsorption sites on the $Zn_4O(CO_2)_6$ and the C_6H_4 units of MOF-5 and uncover edgewise C_6H_4···Ar and C_6H_4···N_2 interactions previously unknown in gas-phase studies of aromatic van der Waals complexes.

Diffraction-quality single crystals of MOF-5 were produced by the solvothermal reaction of zinc nitrate with terephthalic acid in *N*,*N*-diethylformamide (*16*). The material used in the present study was initially evacuated ($<10^{-3}$ Torr) of any gas or volatiles, and its stability was checked by thermal gravimetric analysis, which revealed a large temperature range (100° to 470°C) of stability with no observable weight loss (Fig. 1). The crystal specimens were mounted in capillaries connected to a gas manifold for evacuation before being backfilled with Ar or N_2 and flame-sealed. The amount of gas available for adsorption was estimated from the backfill pressure, crystal size, and the dimensions of the capillaries to be about 5 to 10 gas molecules per formula unit of MOF-5, $Zn_4O(BDC)_3$ (BDC is 1,4-benzenedicarboxylate), which is less than half the established saturation uptake for MOF-5 (*4*).

XRD data were collected by using a single crystal diffractometer equipped with a charge-coupled device camera and an open-flow helium cryostat at temperatures between 293 and 30 K (*16*, *17*). To confirm the completeness of the evacuation procedure, we collected data at 30 K on a single crystal of MOF-5 sealed under vacuum. Refinement of these data confirmed the maintainance of the cubic symmetry of MOF-5 and the absence of guest molecules in the pores (largest electron density peak and hole were 0.444 and –0.238 $e^-/Å^3$, respectively) as shown in the thermal ellipsoid plot of Fig. 2A.

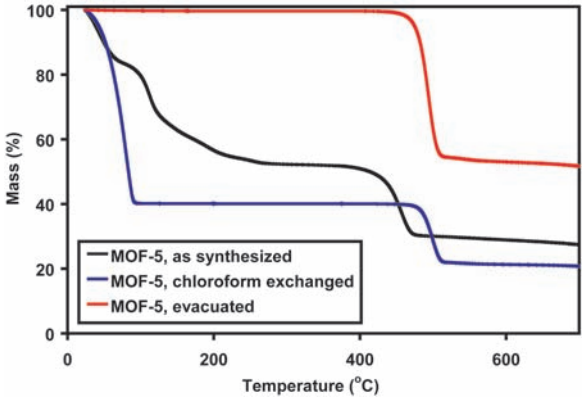

Fig. 1. Thermal behavior of MOF-5 in the as-synthesized, chloroform-exchanged, and evacuated states. The as-synthesized material (black trace) displays a multistep weight loss of 48% up to 300°C, attributed to the desorption of 7.0 *N*,*N*-diethylformamide molecules per formula unit before the onset of decomposition at 410°C. In contrast, the chloroform guests in the exchanged material (blue trace) are completely removed by 100°C (60% weight loss, equivalent to 9.7 chloroform molecules per formula unit). The evacuated framework (red trace) shows no weight loss to 470°C.

Further XRD data were collected from crystals of MOF-5 loaded with Ar or N_2 between 293 and 30 K. Refinement of data collected at 293 K revealed no significant peaks of electron density attributable to guests in the extra-framework region in either case, as would be expected from their weak interaction (Fig. 2, B and C). As the temperature was lowered, many local maxima were located in the observed structure factor (F_{obs}) Fourier maps, providing evidence of the localization of the gas atoms. This localization is most apparent at 30 K in the regions proximal to the $Zn_4O(CO_2)_6$ unit. The shape and amplitude of the electron density contours of Ar and N_2 atoms near this unit are shown in Fig. 2, D and E, respectively. This first site, denoted $\alpha(CO_2)_3$, lies on a triangular face of the octahedron whose vertices are defined by the carboxylate C atoms. This site (Wyckoff site 32*f*, *x* coordinate ~ 0.34) exhibits the highest occupancy in all refinements over the temperature range examined and can be identified as the primary adsorption site. Its symmetry allows the adsorption of up to four adsorbates per formula unit. At this site, the curvature is higher than anywhere else on the framework surface, which allows the adsorbates to interact with three carboxylates and three Zn atoms. The Zn–O and C–O dipoles are presumably most effective in polarizing the gas atoms and lead to comparatively strong interactions.

An additional seven adsorption sites were identified from local maxima of electron density, which are partially occupied by Ar at 30 K. In total, there are five primary adsorption sites, including $\alpha(CO_2)_3$, that are closest to the framework, and three secondary ones that form a second layer of adsorption in the pores (Fig. 3,

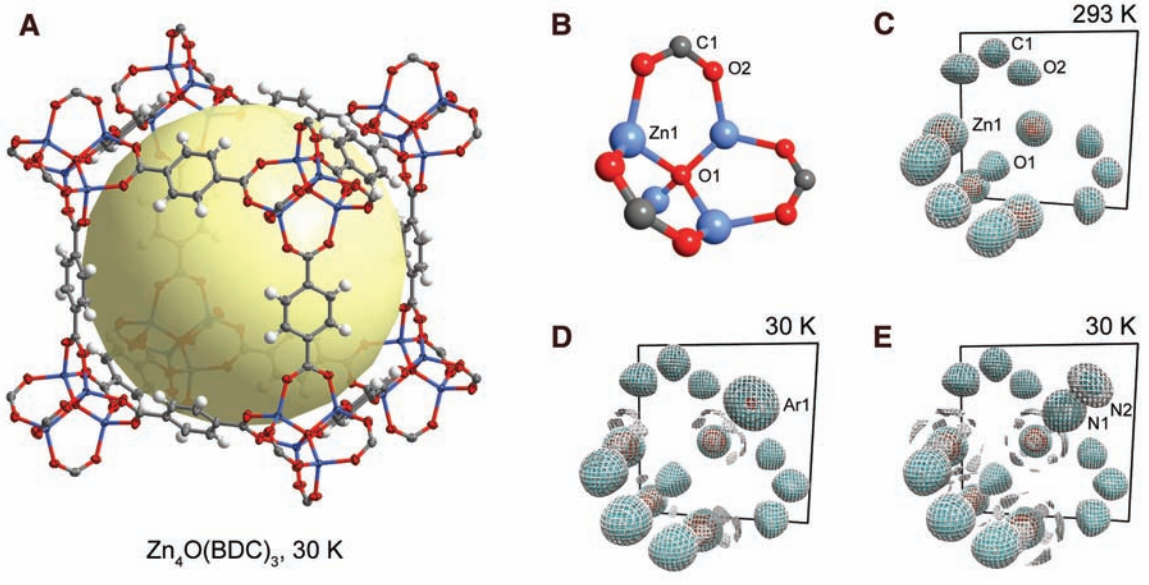

Fig. 2. (**A**) The MOF-5 structure consists of a cubic array of $Zn_4O(CO_2)_6$ units connected by phenylene links (atoms shown as thermal ellipsoids of 90% probability: C, black; H, white; O, red; and Zn, blue), which define large pseudocubic pores that can be completely evacuated. The yellow sphere represents the largest sphere that can occupy the pore without contacting the van der Waals surface of the framework. (**B**) A magnification of the corner of the pore schematically shows the location of adsorption site $\alpha(CO_2)_3$, located equidistant to the three carboxylates. (**C**) The corresponding three-dimensional electron density map (F_{obs}) of this site, determined from single-crystal XRD data obtained at 293 K from crystals loaded under either N_2 or Ar. Only regions of electron density assigned to the framework atoms shown in (**B**) are observed. At 30 K, regions of electron density assigned to adsorbed (**D**) Ar or (**E**) N_2 become prominent. At 30 K, Fourier ripples around the Zn atoms can also be observed. Contours ($e^-/Å^3$): silver, >3; blue, >10; red, >60.

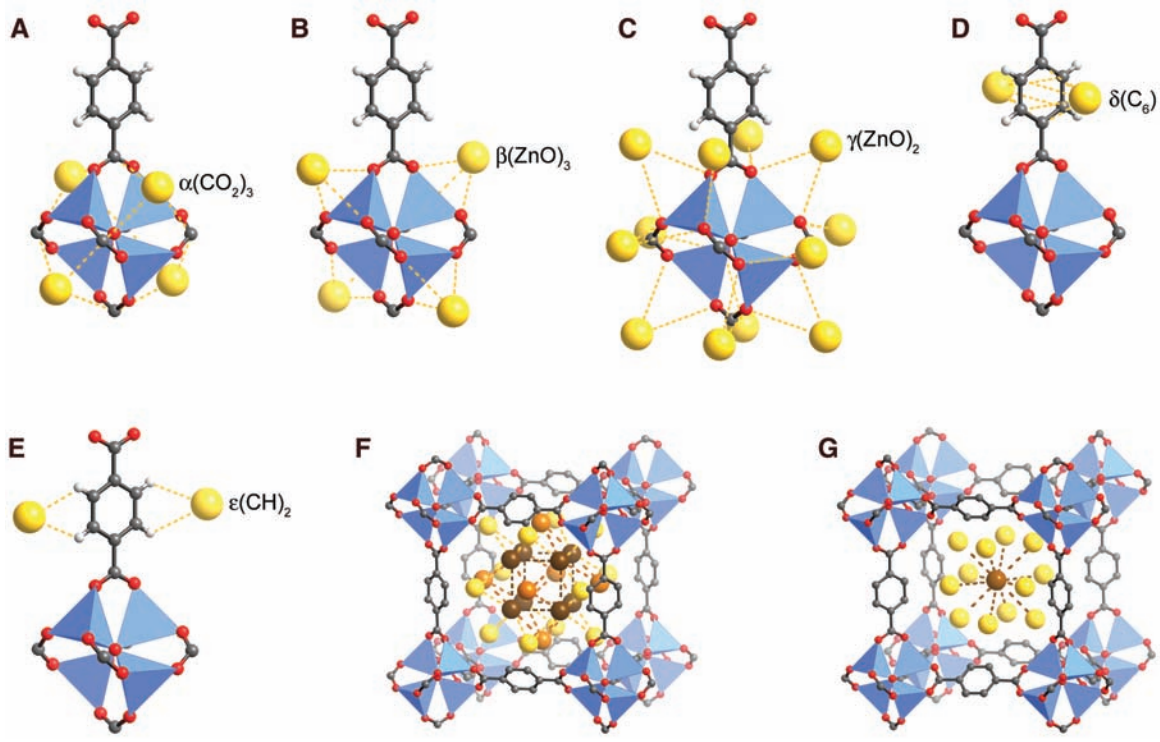

Fig. 3. At 30 K, eight symmetry-independent sites are crystallographically identified as partially occupied by Ar atoms (shown as yellow spheres) in the pores of MOF-5. These include (**A** to **C**) three sites primarily associated with the secondary building unit and those above the (**D**) face and (**E**) edges of the linker. Sites are labeled according to the description in the text. (**F**) Sites ϕ (orange spheres) and η (brown spheres) form a second layer in the large pore above site $\delta(C_6)$ (yellow spheres); (**G**) site θ (brown sphere) is located at the center of the small pore surrounded by site $\varepsilon(CH)_2$ (yellow spheres).

Table 1. Important interatomic distances for Ar adsorbed in MOF-5 at 30 K. Atomic labels correspond to those used in the crystallographic refinements, and primes indicate symmetry equivalents. Dashed entries indicate no close framework contacts.

Adsorption site	Closest framework contacts (Å)		Intersite distances (Å)	
$\alpha(CO_2)_3$	Three Ar(1)···C(1)	3.572	$\alpha(CO_2)_3$···$\gamma(ZnO)_2$	3.677
	Six Ar(1)···O(2)	3.601	$\alpha(CO_2)_3$···η	3.828
	Three Ar(1)···Zn(1)	3.926		
$\beta(ZnO)_3$	Three Ar(2)···O(2)	3.492	$\beta(ZnO)_3$···$\varepsilon(CH)_2$	3.270
	Three Ar(2)···H(3)	3.281	$\beta(ZnO)_3$···$\gamma(ZnO)_2$	3.471
	One Ar(2)···Zn(1)	3.686		
$\gamma(ZnO)_2$	Two Ar(3)···O(2)	3.792	$\gamma(ZnO)_2$···$\beta(ZnO)_3$	3.471
	Two Ar(3)···H(3)	3.306	$\gamma(ZnO)_2$···$\alpha(CO_2)_3$	3.677
			$\gamma(ZnO)_2$···ϕ	3.729
			$\gamma(ZnO)_2$···$\delta(C_6)$	3.820
			$\gamma(ZnO)_2$···$\varepsilon(CH)_2$	3.968
$\delta(C_6)$	Three Ar(4)···C(2)	3.635	$\delta(C_6)$···η	3.652
	Three Ar(4)···C(3)	3.639	$\delta(C_6)$···$\gamma(ZnO)_2$	3.820
			$\delta(C_6)$···ϕ	4.112
$\varepsilon(CH)_2$	Two Ar(5)···H(3)	3.288	$\varepsilon(CH)_2$···$\beta(ZnO)_3$	3.270
			$\varepsilon(CH)_2$···$\varepsilon(CH)_2$	3.770
			$\varepsilon(CH)_2$···$\gamma(ZnO)_2$	3.968
			$\varepsilon(CH)_2$···θ	4.073
ϕ	—		ϕ···η	3.716
			ϕ···$\gamma(ZnO)_2$	3.729
			ϕ···$\delta(C_6)$	4.112
η	—		η···$\delta(C_6)$	3.652
			η···ϕ	3.716
			η···η'	3.763
			η···$\alpha(CO_2)_3$	3.828
θ	—		θ···$\varepsilon(CH)_2$	4.073

A to G). Their respective distances from framework atoms and adjacent sites are summarized in Table 1. In addition to $\alpha(CO_2)_3$, the primary sites include the site above the face of a ZnO_4 tetrahedron, $\beta(ZnO)_3$; the site above the edge of a ZnO_4 tetrahedron, $\gamma(ZnO)_2$; the site above the C_6H_4 phenylene face, $\delta(C_6)$; and the site on the phenylene edge, $\varepsilon(CH)_2$. Two additional sites were observed in the large pore, ϕ and η, as well as a third secondary site at the center of the pore, θ.

The known difficulties associated with the high correlation of site occupancy and thermal displacement parameters were carefully considered, and comparison of the peak heights at these positions with those of the framework atoms in the F_{obs} Fourier maps allowed atomic assignments and subsequent convergence of the least squares refinement with acceptable statistics (*16*). Unlike $\alpha(CO_2)_3$, the remaining seven adsorption sites exhibit smaller relative occupancies, indicating that the binding energies at these sites are similar and less than those at $\alpha(CO_2)_3$. The small occupancies (10 to 20%) of some of these sites reflects the limiting amount of Ar in the capillary; however, it must be noted also that any two sites separated by less than the sum of the van der Waals radii cannot be simultaneously occupied in any one unit cell. For Ar, the nearest neighbor separation of 3.76 Å is taken from the structure of its solid phase (*18*). We note that Ar packing at all adsorption sites (Fig. 3) is not appropriate for all unit cells. At full capacity (28.8 Ar per formula unit) (*4*), it would be necessary to invoke a highly disordered model. One packing arrangement might involve full occupation of sites $\alpha(CO_2)_3$, $\delta(C_6)$, $\varepsilon(CH)_2$, η, and θ and 70% filling of site $\gamma(ZnO)_2$ (corresponding to 28.9 Ar per formula unit), but this model also requires some positional disorder from the high symmetry sites.

Evidence that these sites are intrinsic to MOF-5 was provided by the adsorption of N_2 and our ability to readily observe the adsorption sites from the XRD data, which were determined to be the same as those found for Ar. Even at a temperature as high as 120 K, significant electron density was located at the primary adsorption site $\alpha(CO_2)_3$. At 30 K, the two distinct atoms of the N_2 molecule can be

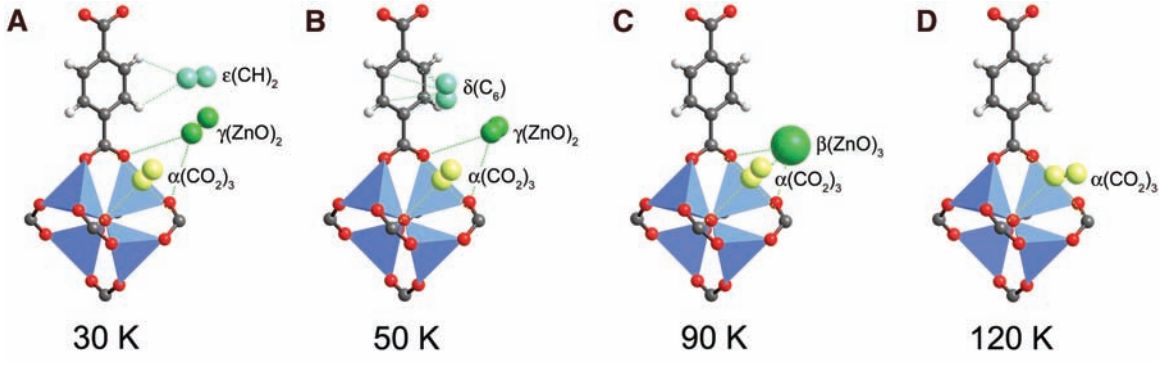

Fig. 4. (**A**) At 30 K, three independent sites are partially occupied by N_2 molecules in the pores of MOF-5, which correspond to sites $\alpha(CO_2)_3$, $\gamma(ZnO)_2$, and $\varepsilon(CH)_2$ of the Ar-loaded structure. Relevant interatomic distances from closest N atom to framework atoms (in Å) include: site $\alpha(CO_2)_3$, 3 C at 3.379, 6 O at 3.372, 3 Zn at 3.606; $\gamma(ZnO)_2$, 2 O at 3.668, 2 H at 3.244; $\varepsilon(CH)_2$, 2 H at 3.097. Intersite distances (measured between molecular centers of mass): $\alpha(CO_2)_3$-$\gamma(ZnO)_2$, 4.104; $\gamma(ZnO)_2$-$\varepsilon(CH)_2$, 4.026; and $\varepsilon(CH)_2$-$\varepsilon(CH)_2'$, 3.708. (**B**) As the temperature is increased, the relative occupancy of these sites changes such that at 50 K site $\delta(C_6)$ is occupied instead of $\varepsilon(CH)_2$; (**C**) at 90 K, site $\beta(ZnO)_3$ is occupied instead of $\gamma(ZnO)_2$, $\delta(C_6)$, or $\varepsilon(CH)_2$; (**D**) at 120 K, only site $\alpha(CO_2)_3$ was occupied. Where refinement was possible, N_2 molecules are shown as their individual atoms, but at 90 K N_2 molecules on site $\beta(ZnO)_3$ appear to be rotationally disordered, and at 120 K there are three possible orientations for N_2 on site $\alpha(CO_2)_3$ (only one is shown).

modeled at three adsorption sites equivalent to $\alpha(CO_2)_3$, $\gamma(ZnO)_2$, and $\varepsilon(CH)_2$ of the Ar-loaded structure (Fig. 4A). For site $\alpha(CO_2)_3$, the molecule is aligned with the threefold axis, allowing a closer approach of one atom (N1) to the framework. Site $\gamma(ZnO)_2$ is also strongly associated with the inorganic cluster, interacting with two separate carboxylate O atoms and two H atoms of the phenylene links. There are 12 of these sites per formula unit (Wyckoff site 96*k*). Site $\varepsilon(CH)_2$ is located at the edges of the phenylene links, and there are six of these per formula unit (Wyckoff site 48*h*). The nearest neighbor (center of mass) distances between sites $\alpha(CO_2)_3$, $\gamma(ZnO)_2$, and $\varepsilon(CH)_2$ are similar to those found in the solid N_2 phases [3.79 to 4.05 Å (*19*)], the dense quadrupolar-ordered phase of N_2 on graphite [4.04 Å (*20*)], and the high-order commensurate structure of N_2 on MgO(100) [3.58 Å (*21*)].

As the temperature is increased to 50 K, site $\delta(C_6)$ is occupied but site $\varepsilon(CH)_2$ is not (Fig. 4B). At 90 K, sites $\gamma(ZnO)_2$, $\delta(C_6)$, and $\varepsilon(CH)_2$ do not show appreciable occupancy; instead, it is primarily at sites $\alpha(CO_2)_3$ and $\beta(ZnO)_3$ (Fig. 4C). At 120 K, only site $\alpha(CO_2)_3$ is partially occupied (Fig. 4D). These results imply a qualitative relation in terms of energy of adsorption for the sites in the order $\alpha(CO_2)_3 \gg \beta(ZnO)_3 > \gamma(ZnO)_2 > \delta(C_6) \sim \varepsilon(CH)_2$. Packing effects cannot be ignored; the separation of the $\beta(ZnO)_3$ and $\gamma(ZnO)_2$ sites is too small for them to be simultaneously occupied, and because $\gamma(ZnO)_2$ has a greater multiplicity (i.e., greater capacity per formula unit), it may become the more important site of the two at lower temperatures to accommodate further adsorbate. The lack of observable electron density at sites ϕ, η, and θ may be attributed to the lesser tendency for N_2 to create an ordered second layer at this small loading.

Our ability to observe and determine the sequential adsorption of gases at well-defined and multiple sites within the large pores of MOF-5 contrasts with other studies performed on molecular materials with much smaller cavities or constricted channels (*14*, *15*, *22*–*24*). In such cases, gases are confined by the narrowness of the pores, and the systems lack the potential for fine-tuning the steric and electronic attributes of the adsorption sites. The openness of MOF-5, however, gives adsorption sites that exhibit partial occupancies through factors related to guests reversibly adsorbing and desorbing and migrating between adjacent sites and the inability to occupy simultaneously sites that are separated by less than the sum of the guests' van der Waals radii. It is not possible to distinguish between these cases with XRD data because they correspond to a time-averaged view of the gas behavior. However, related experimental and theoretical work on small guest molecules in zeolites suggest that each of these situations do occur as a function of temperature (*25*–*28*).

Nevertheless, the presence of multiple adsorption sites in MOF-5 and our ability to precisely locate their positions leads to a rare insight into MOF structures. Specifically, the C_6 phenylene rings are profoundly altered by the presence of the zinc oxide units as evidenced by the observation of Ar and N_2 adsorption sites on the edges of the phenylene ring, $\varepsilon(CH)_2$; a mode, unlike that of the phenylene face, $\delta(C_6)$, previously unobserved in the gas-phase studies of van der Waals complexes of gases with benzene (*29*, *30*). As the MOF-5 structure shows (Fig. 2A), one finds that each C_6 ring is attached to two six-membered rings of –O–C–O–Zn–O–Zn– composition. These heterorings are coplanar to the C_6 ring and undoubtedly alter its electronic character relative to C_6 rings of free benzene, graphite, and carbon nanotubes. Confinement effects enhancing adsorbate-adsorbate interactions may also contribute to the stabilization of binding at these edge sites.

Our findings here also shed some light on the basis for H_2 binding in MOFs. Analysis of INS data collected from MOF-5 as a function of H_2 loading suggested that the favored binding site was near the inorganic secondary building unit (*9*). Additional molecules would then occupy sites closer to or (lastly) on the organic linkers as the loading is increased. However, single-site occupation was not observed in the INS study even at the lowest loading of four H_2 molecules per formula unit, which is equal to the crystallographic multiplicity of this site. This situation is similar to the case in zeolites and suggests that the corrugation of the potential energy surfaces for binding of these molecules is very small. The present study corroborates the qualitative picture developed from the INS studies and provides the missing details of the adsorption sites (Figs. 2 to 4).

The recorded increase of ~200 $Å^3$ (1%) in the unit cell volumes of the materials upon decreasing the temperature from 293 to 30 K suggests that the framework may exhibit negative thermal expansion (*31*). This possibility is being investigated in greater detail by further multitemperature experiments.

References and Notes

1. M. Eddaoudi *et al.*, *Science* **295**, 469 (2002).
2. S. Kitagawa, R. Kitaura, S.-I. Noro, *Angew. Chem. Int. Ed. Engl.* **43**, 2334 (2004).
3. O. M. Yaghi *et al.*, *Nature* **423**, 705 (2003).
4. H. Li, M. Eddaoudi, M. O'Keeffe, O. M. Yaghi, *Nature* **402**, 276 (1999).
5. H. K. Chae *et al.*, *Nature* **427**, 523 (2004).
6. G. Férey *et al.*, *Angew. Chem. Int. Ed. Engl.* **43**, 6296 (2004).
7. S.-I. Noro, S. Kitagawa, M. Kondo, K. Seki, *Angew. Chem. Int. Ed. Engl.* **39**, 2082 (2000).
8. K. Seki, W. Mori, *J. Phys. Chem. B* **106**, 1380 (2002).
9. N. L. Rosi *et al.*, *Science* **300**, 1127 (2003).
10. G. Férey *et al.*, *Chem. Comm.* **2003**, 2976 (2003).
11. D. N. Dybtsev, H. Chun, S. H. Yoon, D. Kim, K. Kim, *J. Am. Chem. Soc.* **126**, 32 (2004).
12. J. L. C. Rowsell, A. R. Millward, K. S. Park, O. M. Yaghi, *J. Am. Chem. Soc.* **126**, 5666 (2004).
13. A. Zecchina, C. Otero Areán, *Chem. Soc. Rev.* **25**, 187 (1996).
14. R. Kitaura *et al.*, *Science* **298**, 2358 (2002).
15. Y. Kubota *et al.*, *Angew. Chem. Int. Ed. Engl.* **44**, 920 (2005).
16. Materials and methods are available as supporting material on *Science* Online. All structures are cubic, space group $Fm\bar{3}m$, $a \sim 25.8$ Å, $Z = 8$. The cell parameter of the N_2-loaded structure varies between 25.794 ± 0.004 Å at 293 K and 25.898 ± 0.004 Å at 30 K. Results of the refinements of the evacuated,

Ar-loaded and N_2-loaded crystal structures (in CIF format) have been deposited as CCDC 277428-277437. These data can be obtained free of charge via www.ccdc.cam.ac.uk/conts/retrieving.html [or from the Cambridge Crystallographic Data Centre, 12 Union Road, Cambridge CB21EZ, UK; fax, (+44)1223-336-033; or deposit@ccdc.cam.ac.uk].
17. A. E. Goeta, J. A. K. Howard, *Chem. Soc. Rev.* **33**, 490 (2004).
18. C. S. Barrett, L. Meyer, *J. Chem. Phys.* **41**, 1078 (1964).
19. A. F. Schuch, R. L. Mills, *J. Chem. Phys.* **52**, 6000 (1970).
20. J. Eckert, W. D. Ellenson, J. B. Hastings, L. Passell, *Phys. Rev. Lett.* **43**, 1329 (1979).
21. M. Trabelsi, J. P. Coulomb, D. Degenhardt, H. Lauter, *Surf. Sci.* **377–379**, 38 (1997).
22. E. D. Sloan Jr., *Clathrate Hydrates of Natural Gases* (Dekker, New York, ed. 2, 1998), ch. 2.
23. S. Takamizawa, E. I. Nakata, H. Yokoyama, K. Mochizuki, W. Mori, *Angew. Chem. Int. Ed. Engl.* **42**, 4331 (2003).
24. J. L. Atwood, L. J. Barbour, A. Jerga, *Science* **296**, 2367 (2002); published online 9 May 2002 (10.1126/science.1072252).
25. C.-R. Anderson, D. F. Coker, J. Eckert, A. L. R. Bug, *J. Chem. Phys.* **111**, 7599 (1999).
26. J. A. McKinnon, D. F. Coker, J. Eckert, A. L. R. Bug, *J. Chem. Phys.* **114**, 10137 (2001).
27. R. Kahn, E. Cohen de Lara, E. Viennet, *J. Chem. Phys.* **91**, 5097 (1989).
28. E. Cohen de Lara, R. Kahn, *Zeolites* **12**, 256 (1992).
29. R. Nowak, J. A. Menapace, E. R. Bernstein, *J. Chem. Phys.* **89**, 1309 (1988).
30. T. Weber, A. von Bargen, E. Riedle, H. J. Neusser, *J. Chem. Phys.* **92**, 90 (1990).
31. J. S. O. Evans, *Dalton Trans.* **1999**, 3317 (1999).
32. Supported by NSF, U.S. Department of Energy (O.M.Y.), the Link Foundation, Natural Sciences and Engineering Research Council of Canada (J.L.C.R.), the Institut Laue-Langevin (E.C.S.), and the Engineering and Physical Sciences Research Council (Senior Research Fellowship, J.A.K.H.). We thank G. J. McIntyre (Institut Laue-Langevin) for helpful discussions.

Supporting Online Material
www.sciencemag.org/cgi/content/full/309/5739/1350/DC1
Materials and Methods
Figs. S1 to S3

6 April 2005; accepted 21 July 2005
10.1126/science.1113247

High Frictional Anisotropy of Periodic and Aperiodic Directions on a Quasicrystal Surface

Jeong Young Park,[1] D. F. Ogletree,[1] M. Salmeron,[1]* R. A. Ribeiro,[2] P. C. Canfield,[2] C. J. Jenks,[2] P. A. Thiel[2]

Strong friction anisotropy is found when the twofold surface of an atomically clean aluminum-nickel-cobalt quasicrystal slides against a thiol-passivated titanium-nitride tip. Friction along the aperiodic direction is one-eighth as much as that along the periodic direction. This anisotropy, which is about three times as large as the highest value observed in anisotropic crystalline surfaces, disappears after the surface is oxidized in air. These results reveal a strong connection between interface atomic structure and the mechanisms by which energy is dissipated, which likely include electronic or phononic contributions, or both.

The origin of friction and the energy dissipation mechanisms that underlie it are still being explored in fundamental studies. To this day, simple ideas from the times of Leonardo da Vinci, such as the existence of a strong connection between the geometric corrugation profiles (even at the atomic scale) of two contacting surfaces, are still invoked to explain friction (*1*). The idea is that commensurability leads to intimate interlocking and high friction, whereas incommensurability leads to low friction, because the two materials do not come into registry at any length scale. Some of these ideas have been verified recently by rubbing two surfaces of graphite or mica against each other (*2*, *3*) under conditions where wear and plastic deformation are minimized, so that fundamental dissipation forces can be explored. Friction was found to be largest when the crystallographic orientation of the two identical surfaces coincided. Commensurability, however, is only one aspect of the friction problem and does not apply to most interfaces, because the contacting materials are different and therefore almost always incommensurate. Friction anisotropy between incommensurate surfaces has been observed when at least one of the surfaces is crystalline and anisotropic, i.e., when the periodicity changes in different directions. This anisotropy is typically less than a factor of 2 (*4*), although in the case of some organic monolayers on mica, a factor of 3 was observed (*5*).

A different question is whether the existence of periodicity itself is important in friction. For example, it is in periodic systems that the highest thermal and electrical conductivities are found. To explore this question, one could compare the friction properties of a material prepared in crystalline and amorphous forms. This, however, is very difficult, because the two surfaces of the material are likely to be chemically different, which would change the friction properties. As we discuss below, our quasicrystal surface provides a unique example of a material where the periodicity exists only in one direction.

Quasicrystal intermetallics (*6*, *7*), which have long-range atomic order but no periodicity, are ideal samples for exploring this idea, because in two-dimensional quasicrystals, such as decagonal Al-Ni-Co, certain surface terminations exhibit periodic as well as aperiodic atomic ordering along different directions. Quasicrystal surfaces, which are oxidized under ambient conditions, are already known for their high hardness and low friction (*8*–*12*), although these results were obtained under conditions where plastic deformation occurred during sliding. To investigate fundamental aspects of friction on quasicrystals, we cut an Al-Ni-Co single quasicrystal perpendicular to its 10-fold rotational axis to produce a surface

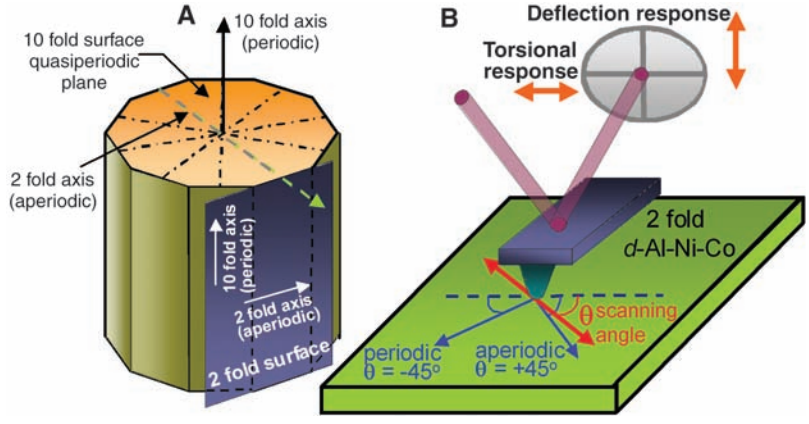

Fig. 1. (**A**) Schematic model of a decagonal Al-Ni-Co quasicrystal, showing the orientation of decagonal and twofold planes. The 2-fold plane is periodic along the 10-fold direction and aperiodic along the 2-fold direction. (**B**) Schematic of the cantilever and the scanning geometry during friction studies.

[1]Materials Sciences Division, Lawrence Berkeley National Laboratory, University of California, Berkeley, CA 94720, USA. [2]Ames Laboratory and Departments of Chemistry, Physics and Astronomy, and Materials Science and Engineering, Iowa State University, Ames, IA 50011, USA.

*To whom correspondence should be addressed. E-mail: mbsalmeron@lbl.gov